Time courses of strains that induce necking and fracturing in high-density polyethylene

Shengwang Hao [a,*], Xinyue Wu [a], Chunsheng Lu [b]

[a] *School of Civil Engineering and Mechanics, Yanshan University, Qinhuangdao, China*
[b] *School of Civil and Mechanical Engineering, Curtin University, Perth, Australia*

A R T I C L E I N F O

A B S T R A C T

High-density polyethylene is widely used in pressure pipe applications, but its necking and pre-cut effects are still poorly understood. Herein, we analyze the spatial distributions of the time courses of strains to highlight the strain field evolution to necking and the effect of pre-cutting on the strain field evolution in a high-density polyethylene material deformed under tension. Digital image correlation was used to measure the strain fields on two perpendicular surfaces of a specimen. Necking and its propagation in the tension direction dominate the failure behavior of an intact specimen. However, in the pre-cut specimen, crack propagation prevents neck propagation in the tension direction. Energy release outside the crack zone is observed as a decrease in strain at approximately the failure time. This leads to a macroscopic stress-strain curve that deviates from that of the intact specimen. These findings provide novel insights that are significant in the theoretical modelling and simulations of advanced polymeric materials and structures.

1. Introduction

High-density polyethylene (HDPE) pipes are widely used in civil infrastructure and environmental engineering projects, such as urban gas and water systems, because of their advantages of low masses and costs, high fracture toughnesses, and corrosion resistances [1]. Recognizing the deformation and failure processes of HDPE materials is fundamental in modelling their constitutive behaviors and designing relevant structures. Thus, substantial studies have been performed to determine the evolution properties of their stress-strain responses, fracture toughnesses, and time-dependent behaviors. The failure mechanisms of HDPE materials, including necking, localized deformation and damage propagations, are complicated. However, studies regarding the heterogeneous, evolving properties of strains at certain spatial positions and their relationships with macroscopic responses are still lacking.

The plastic instabilities of HDPE materials are key in evolving deformations that induce failures. Under uniaxial tension, necking is typically defined as an indicator of the plastic instability [2–5] of a polymeric material. Strain field measurements using digital image correlation (DIC) [6] indicated that strains are significantly localized when the macroscopic strain exceeds the elastic limit and that deformation in

a necked HDPE specimen is strongly anisotropic. After necking, deformation is highly concentrated in the necking region, and the specimen exhibits two parts with different deformation patterns. Consequently, the macroscopic average quantities that define the constitutive behaviors of an HDPE specimen may not be used to describe the subsequent behaviors. Thus, understanding the changes in the spatial strain patterns corresponding to the necking transition is undoubtedly critical in identifying the failure mechanism of an HDPE material and predicting its behavior.

After necking, the strain on the specimen varies with the axial position in the tension direction. Necking and its propagation dominate the behaviors of HDPE materials. Thus, traditional extensometry methods may not efficiently measure the strain rate in a specimen [7], yielding little useful data [8], because only the average strain over the gauge length is measured by tracking the relative positions of two points. Strain localization and necking are general challenges in the fields of experimental mechanics and materials engineering [9,10]. Three-dimensional DIC strain measurements may highlight the dependence of necking on the strain rate [7], but the evolving properties of strain patterns that characterize necking propagation remain an enigma.

DIC is widely used to monitor the deformations of brittle materials, such as rocks [11,12], and analyze the deformation evolution to

---

* Corresponding author.
E-mail address: hsw@ysu.edu.cn (S. Hao).

localization and its propagation properties until failure. The precision of DIC depends on the degree of correlation between the speckle patterns of the reference and target subsets of the deformed sample. A large difference in deformation between the reference and deformed images leads to a decorrelation or mismatch between the two images. In engineering applications, this may be overcome by decreasing the time interval between the two calculated images. A large deformation may then be tracked by acquiring a series of deformed images and performing step-by-step calculations at different stages of loading. These incremental DIC methods have been used by numerous researchers [13–15] in analyzing large deformations. In terms of ductile materials, incremental DIC was used to measure large deformations in rubber [16,17] and polymers [18]. Pan et al. [19] and Zhou et al. [20] proposed two methods of converting relatively large deformations to relatively small deformations using updated reference maps, enabling 3D DIC to yield accurate matching results even in the case of large deformations.

In addition to necking, crack propagation is another key mechanism that leads to the failures of HDPE materials and is crucial in the packaging and transportation of dangerous goods. Practical polymeric structures, such as pipelines and pressure vessels, inevitably contain microcracks within their bodies. Understanding the deformation behaviors of pre-cut polymers is essential in evaluating their safeties and designs and predicting their lifetimes. The presence of a crack may induce brittle fracture in an HDPE pipe, leading to fatal consequences. There is still no standardized method of evaluating crack propagation in polymeric materials. Cracks within polymers drastically change the behaviors of deformations, and the importance of understanding the damage evolution in polymers has been highlighted in numerous studies [21–23]. Damage in polymers has also been studied experimentally [21, 22,24–28], and the results of glassy polymers [21] highlight the effect of volumetric strain on plastic deformation and the contribution of damage to plastic instability.

A displacement-controlled study of a notched specimen is a general method of determining fracture toughness [29,30]. Tension tests of single- or double-edged notched specimens [31,32] are widely used to investigate the effects of cracks on polymer performance. The experimental [33] and numerical [34] results suggest the rate dependences of the fracture processes of polymers. Understanding deformation evolving to failure due to crack propagation in HDPE is key in exploring methods of overcoming the limitations induced by pre-cracks.

Thus, necking and crack propagation, which are the two key factors that dominate the failures of HDPE materials, may be applied to determine the difference in the failure mechanisms of intact and pre-cracked polymer specimens. To date, numerous studies have been conducted regarding the differences in the macroscopic stress-strain curves induced by pre-notches. Substantial efforts have focused on enhancing fracture toughness and decreasing (or eliminating) brittle failure. However, to the best of our knowledge, the changes in the deformation fields that lead to the difference in the average behaviors of intact and pre-cut HDPE specimens are still far from understood.

This study focuses on elucidating the differences between the changes in the strain fields and the failures of intact and pre-cut HDPE specimens. A full-field strain analysis was performed using DIC to simultaneously measure the strain fields at two perpendicular surfaces. This enabled a simultaneous study of the changes in the strain fields at both surfaces, with the pre-cut propagating and opening. Comparing the changes in the strain fields during necking and crack propagation should highlight the differences in their patterns and mechanisms.

2. Materials

The evaluated specimens were prepared using an HDPE-PE100 pipe, which was produced by Hongyue Plastic Group in Qinhuangdao, China. The outer diameter and wall thickness of the pipe were 110 and 10 mm, respectively. The specimens were cut directly along the axial direction of the pipe, according to the GB/T 8804.3–2003 standard [35], as shown in Fig. 1.

The preparation processes of the intact and pre-cut specimens are shown in Fig. 2. To compare the tension behaviors of HDPE materials with and without a pre-cut, two types of specimens, i.e.. pre-cut and intact (non-cut) specimens, were evaluated. A cut with a respective width and depth of 0.23 and 1 mm was manually cut in the middle of the outer wall to yield a pre-cut specimen. The blade, which protruded by 1 mm above the base, was tightly fixed with the edge upward on the base. This instrument was then used to cut the specimens. Thus, the depths and widths of the pre-cuts could be controlled and repeated. The pre-cut thickness was approximately 1/10 of the entire thickness.

3. Experimental methods

As shown in Fig. 3, an Instron 5982 electromechanical universal testing machine (Instron, Norwood, MA, USA) was used in the uniaxial
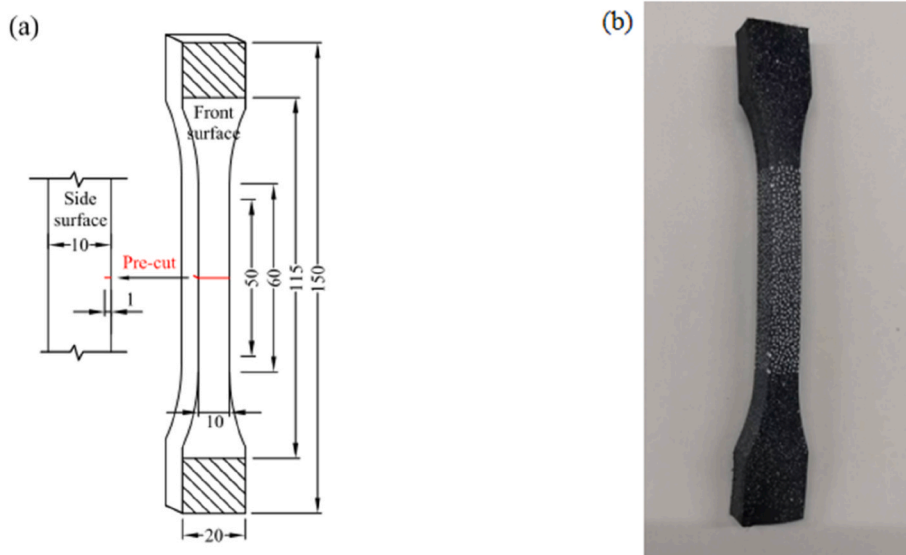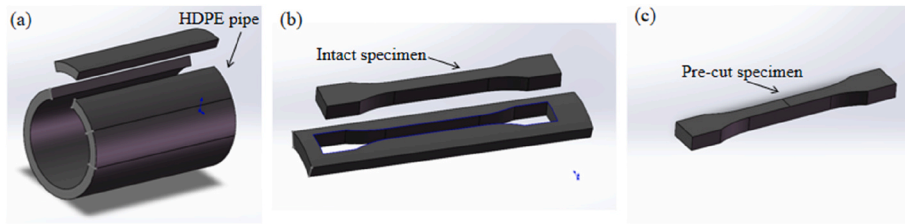

Fig. 1. Geometry and dimensions of a pre-cut high-density polyethylene specimen. (a) Front surface and an enlarged part of the side surface (the units of the numbers are millimeters), and a (b) typical image of a specimen with the artificial speckle pattern.

Fig. 2. Schematic diagram of the preparation of the intact and pre-cut high-density polyethylene (HDPE) specimens. (a) The pipe is cut into several long strips in the axial direction, (b) an intact sample is obtained using a numerically controlled machine tool, and (c) a pre-cut specimen is prepared using a custom-built cutting apparatus.
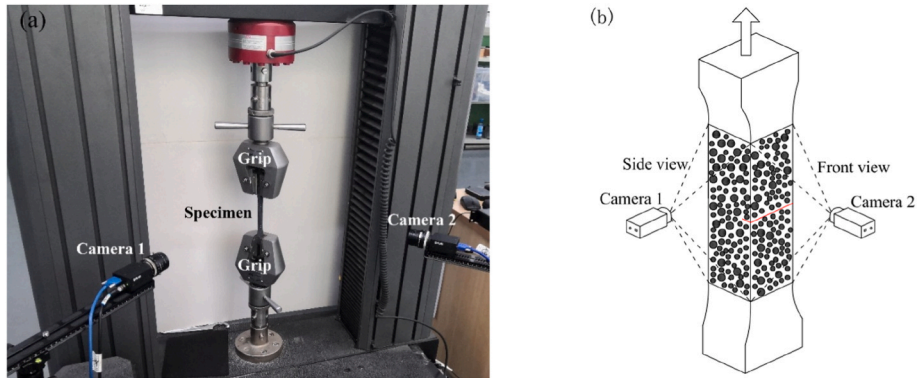

Fig. 3. (a) Image of the experimental setup with stress measurement and digital image correlation systems, and a (b) schematic diagram of an evaluated specimen.

tensile studies and the maximum load measured using the load cell was 100 kN. The accuracy of the tension sensor was 0.0001 N, the specimen was uniaxially stressed at a rate of 3 mm/min, and the acquisition

frequency was 100 Hz.

The surface parallel to the cut front edge is denoted the front surface, and the surface perpendicular to the cut front edge is denoted the side
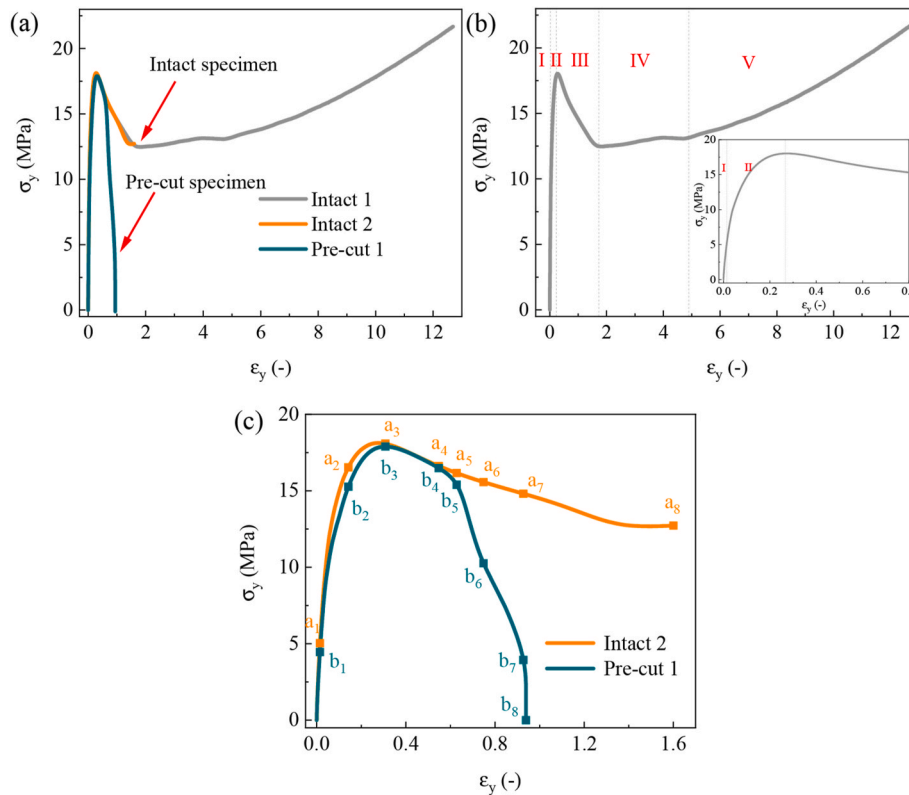
Fig. 4. Engineering stress-strain curves of the intact and pre-cut specimens: (a) entire stress-strain curves of both specimens, (b) five stages of an intact specimen, and (c) magnification of the two curves to show the details of evolution to failure (of the pre-cut specimen) and neck propagation.

surface. The images were captured at frequencies of 5 and 10 Hz with two 2048 × 2048-pixel cameras respectively positioned in front of the two surfaces of the specimen. Artificial speckle patterns were applied to the two surfaces of the specimens (Fig. 1(b)) by spraying with white matte paint, and DIC was used to match the subsets of the two captured images with the speckle patterns. The subsets of deformed images were numerically correlated with the reference subset to determine the full-field surface displacements using the correlation software PMLAB developed by the University of Science and Technology of China (Hefei, China). The subset and step size are two key parameters in the correlation analysis. The subset size is the size of the image window tracked by the correlation algorithm in terms of motion and deformation. The solution provides the displacement components at the center of each subset. The step size is the distance between the centers of the two nearest subsets. In these studies, the subset and step sizes were 29 and 4 pixels, respectively. The displacement fields were determined using the positional differences between the centers of the reference and target subsets with a resolution of ~0.01 pixels and ~50 microstrains.

4. Results

4.1. Stress-strain evolution

Three experiments were performed using each type of specimen, yielding repeatable results. Fig. 4(a) shows three stress-strain curves obtained via the studies (one for each specimen type) under uniaxial tension. The stress-strain evolution in an intact HDPE specimen exhibits five typical stages (Fig. 4(b)). The first stage (I) is characterized by linear elastic behavior. This stage is dominated by the elastic behavior of HDPE, with a homogeneous strain distribution. This is followed by a nonlinear stage (II) until the peak stress point. This stage reveals the degradation of the stiffness due to internal damage, and thus, the effects of the damage are clear. The third stage (III) is characterized by stress softening, which primarily results in damage propagation. The fourth stage (IV) commences when the stress reaches the minimum and then increases slowly. This stage is dominated by viscous behavior and necking propagation. The final stage (V) manifests with fast strain hardening owing to the rapid increase in stress. Strain hardening is mainly caused by induced anisotropy due to molecular chain reorientation. The fracture strength of the intact specimen is higher than its yield strength, which is generally defined as the first peak force point. The intact specimen, with a good toughness, may be extended to a very large length, e.g., the longitudinal engineering strain reaches ~12.68, but the specimen does not fracture. The respective tensile strengths of the intact and pre-cut specimens are 18.07 ± 0.04 and 17.99 ± 0.14 MPa, respectively. The mode I fracture toughness of the pre-cut specimen is $\sim 1.13 \pm 0.01$ MPa m$^{1/2}$.

The pre-cut specimen completely fractures when it is extended to a longitudinal engineering strain of ~0.94. Compared to that of the intact specimen, the small pre-cut significantly changes the tension behavior of HDPE. In the early phase, until point b_4, the pre-cut specimen displays a similar stress-strain curve to that of the intact specimen (until point a_4), as shown in Fig. 4(c). After point b_4, the stress-strain curve of the pre-cut specimen reveals rapid softening, which deviates from the trend of the intact specimen after point a_4.

The entire stress-strain evolution of the pre-cut specimen may be divided into six stages (Fig. 4(c)). The first and second stages are similar to those of the intact specimen and characterized by a linear elastic behavior and nonlinear evolution up to point b_1 and the peak stress point b_3, respectively. The specimen then enters a stress-softening phase characterized by three transitions. The third stage ranges from the peak stress point b_3 (transition to stress softening) to b_4. The specimen subsequently transitions to the fourth stage with rapid softening from point b_4 to b_6. At point b_6, the softening rate reaches the minimum and the stress-strain curve enters the fifth stage. After point b_7, the specimen reaches the failure (sixth) stage, where the softening rate is very sharp, leading to the complete failure of the specimen.

4.2. Changes in shape associated with necking and fracture

Figs. 5 and 6 show the changes in the geometries of both types of specimens, which confirm the changes in the strain fields in terms of neck propagation in the intact specimen and the crack zone in the pre-cut specimen. Necking does not localize in a particular region but propagates along the length. As shown in Fig. 7(a), the cross-sections of the gauge length of an intact specimen are narrowed until almost identical. In contrast, crack propagation and necking occur in the pre-cut specimen, but crack propagation dominates the deformation behavior. The change in the geometry of the front surface of the pre-cut specimen (Figs. 6 and 7(b)) reveals that necking only localizes in the crack zone.

The transverse width of the intact specimen gradually decreases and the longitudinal length is extended. Necking is also observed in the pre-cut specimen during tension, but the length of the neck is small, and finally, fracture occurs. The width of the front surface of the pre-cut specimen (Figs. 6 and 7(b)) narrows because of necking, but finally, the width partially recovers, indicating a transition from necking to dilation. Tearing and propagation of the pre-cut are clearly observed on the side surface of the specimen (Fig. 6).

The intact specimen exhibits clear necking during stretching. It undergoes steady necking expansion after local necking until the cross-section becomes thin over the entire length of the gauge, and the cross-section contraction is ~60%.

4.3. Changes in the strain contours

Notably, in the final phase of tension, the speckle pattern on the surfaces of an intact specimen changes significantly because the specimen is stretched so strongly that the deformation may not be calculated using DIC. Thus, only the strain fields up to point a_8 (Fig. 4(c)) were calculated. In comparison, the entire deformation of the pre-cut specimen is smaller, and the speckle pattern is not destroyed by the deformation. The deformation fields over the entire evaluation of the pre-cut specimen were calculated using DIC.

The horizontal and longitudinal strain contours of the front and side surfaces of the pre-cut specimen are shown in Fig. 8. For comparison, Fig. 9 shows the horizontal and longitudinal strain contours of the intact specimen. In the early phase, the intact and pre-cut specimens (as shown by the strain contours at points b_1 and a_1) exhibit almost homogeneous strain distributions with random, weak spatial fluctuations.

For the pre-cut specimen, at the peak stress point (b_3), the effect of the pre-cut becomes clear, as shown by the strain accumulation around the cut-tip. However, the cut-tip deformation field does not extend to the entire cross-section. The evolution of the stress-strain curve is similar to that of the intact specimen.

After point b_4, the cut-tip deformation field extends to the entire cross-section and thus dominates the cross-sectional deformation behavior, which leads to faster softening. Consequently, the stress-strain curve of the pre-cut specimen begins to deviate from that of the intact specimen. After point a_4, the deformation behaviors of the intact specimen is dominated by necking. The propagation of the necking field dominates the deformation evolution of the phase from a_4 to a_7.

4.4. Time-course distributions of the strains and strain rates associated with necking and fracture

4.4.1. Time-course distributions of the strains and strain rates corresponding to the softening transitions

Figs. 10–12 show the time courses of the strains at different positions along the stretch directions on the front and side surfaces of the intact and pre-cut specimens. In the early phase, the strains at all spatial positions of both specimens increase linearly with time, as shown by the
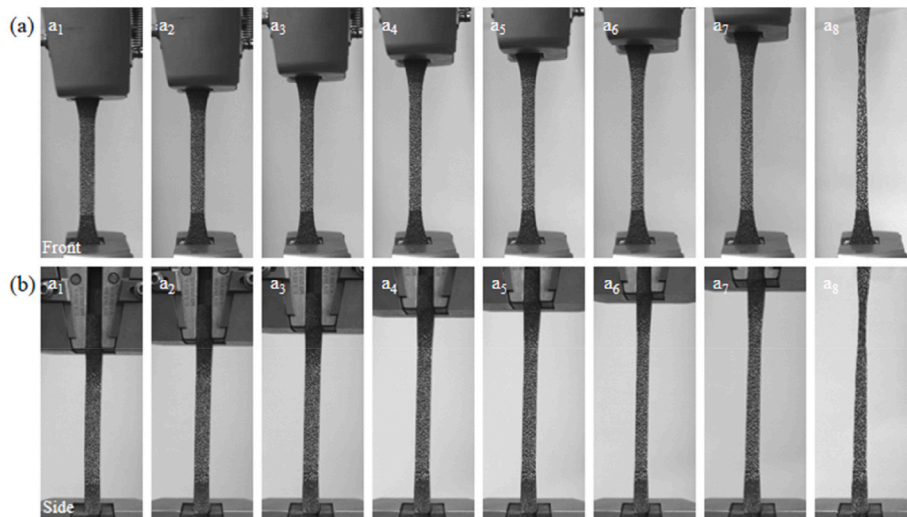
Fig. 5. Images of the changes in the geometry of an intact specimen: the (a) front and (b) side view.
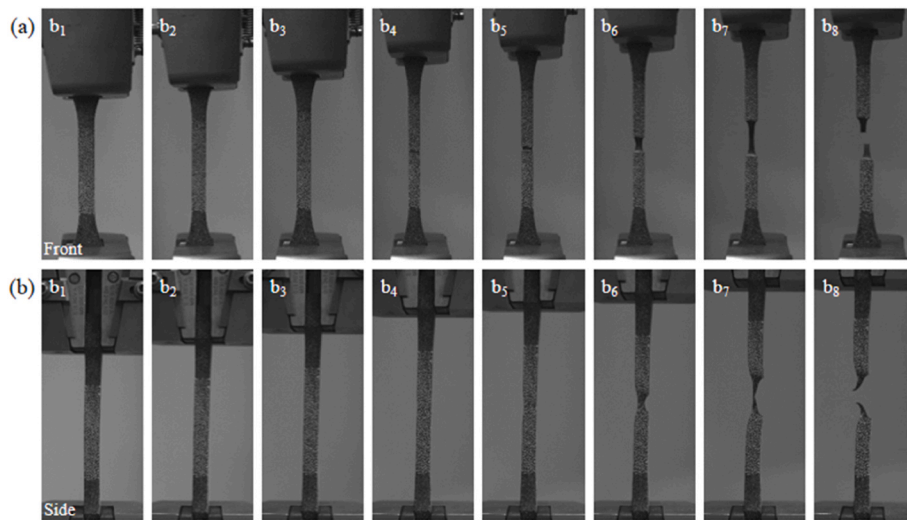

Fig. 6. Images of the changes in the geometry of a pre-cut specimens: the (a) front and (b) side view.
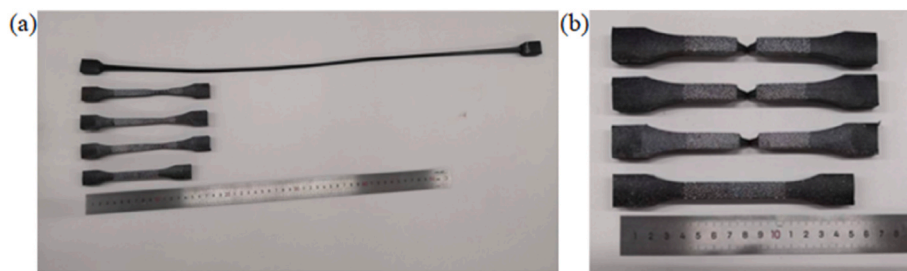

Fig. 7. Images of the changes in the geometries of (a) intact and (b) pre-cut specimens.

constant strain rates (Fig. 13). The strains then increase nonlinearly, but the strains and strain rates remain almost homogeneous, with little difference, up to the peak stress points (Fig. 12). With the softening of the specimens, the spatial distributions of the strains and strain rates become heterogeneous. The strain rates display various accelerations at different spatial positions. Increases in the strains in several areas (e.g., position 1 on the intact specimen shown in Fig. 10 and positions 4 and 5 on the pre-cut specimen shown in Fig. 11(a)) become sharper than those in other areas and these strains exhibit rapid accelerations, although the strain rates at all positions still consistently accelerate. The longitudinal strain on the side surface of the intact specimen is similar to that on the front surface (Fig. 10(b)) and the longitudinal strain increases rapidly at positions 2 and 3 on the side surface of the pre-cut specimen (Fig. 11(b)).

4.4.2. Time-course distributions of the strains and strain rates corresponding to the onset strain of necking in the intact specimen

With the development of heterogeneous deformation fields, the time courses of the strains (Fig. 13(a)) and strain rates (Fig. 13(b)) at different
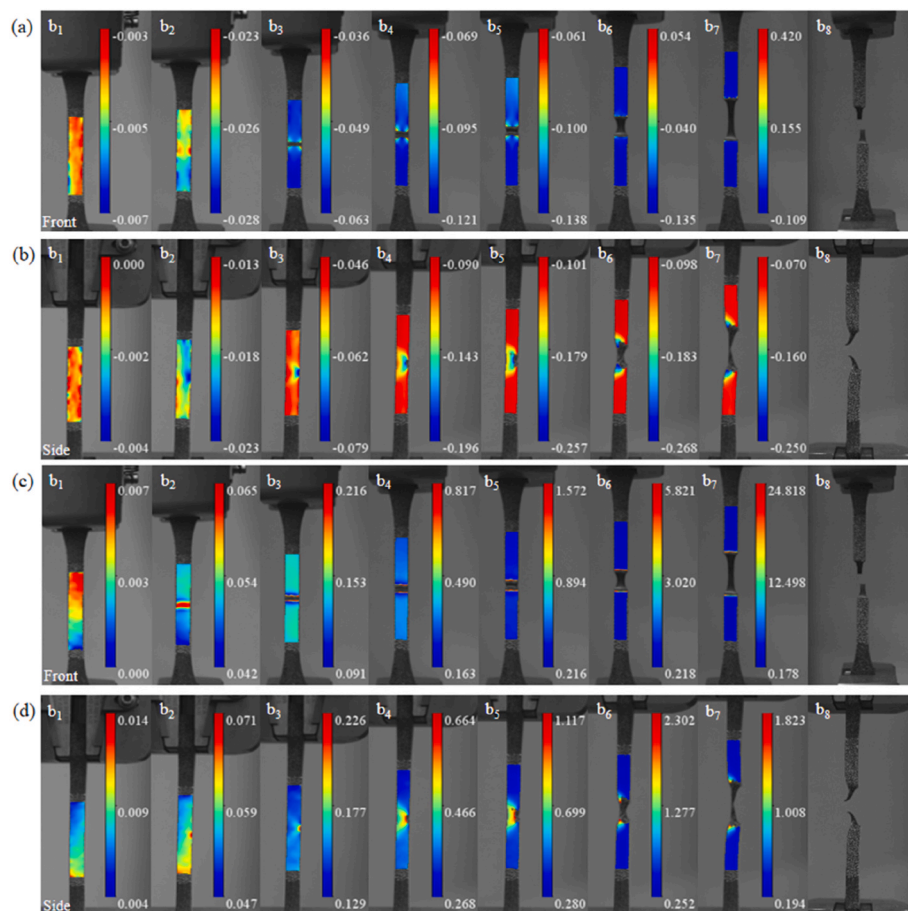
Fig. 8. Strain contours of the two perpendicular surfaces of a pre-cut specimen. (a, c) Front and (b, d) side views of the (a, b) horizontal and (c, d) longitudinal strain.

positions in the stretch direction in an intact specimen display three typical evolving properties after point a_4 in the stress-time curve. Following the earlier linear evolution with time, (i) the strain rate continues to increase, and then decelerates (curve 1 shown in Fig. 13 (b)); (ii) the strain rate increases, then decreases, and then accelerates (curves 2 and 3 shown in Fig. 13(b)); and (iii) the strain rates transitions from acceleration to deceleration until a stable, constant strain state is reached (curves 4 and 5 shown in Fig. 13(b)). Necking nucleates at positions where the strains rate is rapid and the strain rate accelerates monotonically, as indicated by curve 1 shown in Fig. 13(b). In contrast, at other positions, the strain rate transitions from acceleration to deceleration, as shown in Fig. 13(b) (curves 2 and 3). As a result, the strains are localized in the neck zone. This suggests a method of defining the onset engineering strain of necking based on the time course distribution of the strain characterized by the accelerations of the strain rates in the neck region but decelerations of the rates at other positions.

4.4.3. Neck propagation in the intact specimen

With the development of stretching, the strain rates in zones (curves 2 and 3 shown in Fig. 13) adjacent to the initiation position of necking increase following decreases with the initiation of necking. These zones participate in the neck zone, and thus, necking propagates. With neck propagation, the strain rates of the positions in the neck zone decrease, as revealed in the curves shown in Fig. 13 for position 1. However, the strain rates at several positions outside the necking zone, which decelerate with neck propagation, display the third transitions from deceleration to acceleration. These positions participate in the necking zone, and thus, the length of the necking zone increases. During neck propagation, the strain rates at positions far from the necking zone are generally stable with little increase in their strains (curves 4 and 5 shown

in Fig. 13(a)). Their strain rates decrease to almost zero, as revealed by curves 4 and 5 shown in Fig. 13(b), and thus, the stress increases slowly with an almost flat component.

4.4.4. Necking and crack propagation in the pre-cut specimen

In the pre-cut specimen, after the peak stress point, the high longitudinal strain was mainly localized in the zone surrounding the pre-cut (Fig. 11). The strains at positions outside the crack zone began to decrease, which indicated that these regions were unloaded and released elastic deformation energy. This also resulted in rapid accelerations of the strain rates in the crack zone. Softening observed in the strain-time curve became sharp and rapid. Energy release from positions outside the crack zone led to the deviation of the stress-strain curve from that of the intact specimen.

The strains of positions on the same horizontal line in an intact specimen exhibit similar time courses and small differences in strain magnitudes (Fig. 14). However, the time points at which the strains begin to decrease in the pre-cut specimen differ at various positions on the same horizontal line on the front surface (Fig. 15(a)). On the side surface, the strain magnitudes and time points at which the strains begin to decrease display even larger differences (Fig. 15(b)) along the horizontal because of the pre-cut effects. Farther from the cracked surface, transitions occur later, and the magnitudes of the longitudinal strains are smaller.

5. Discussion

5.1. Onset strain point of necking and its propagation

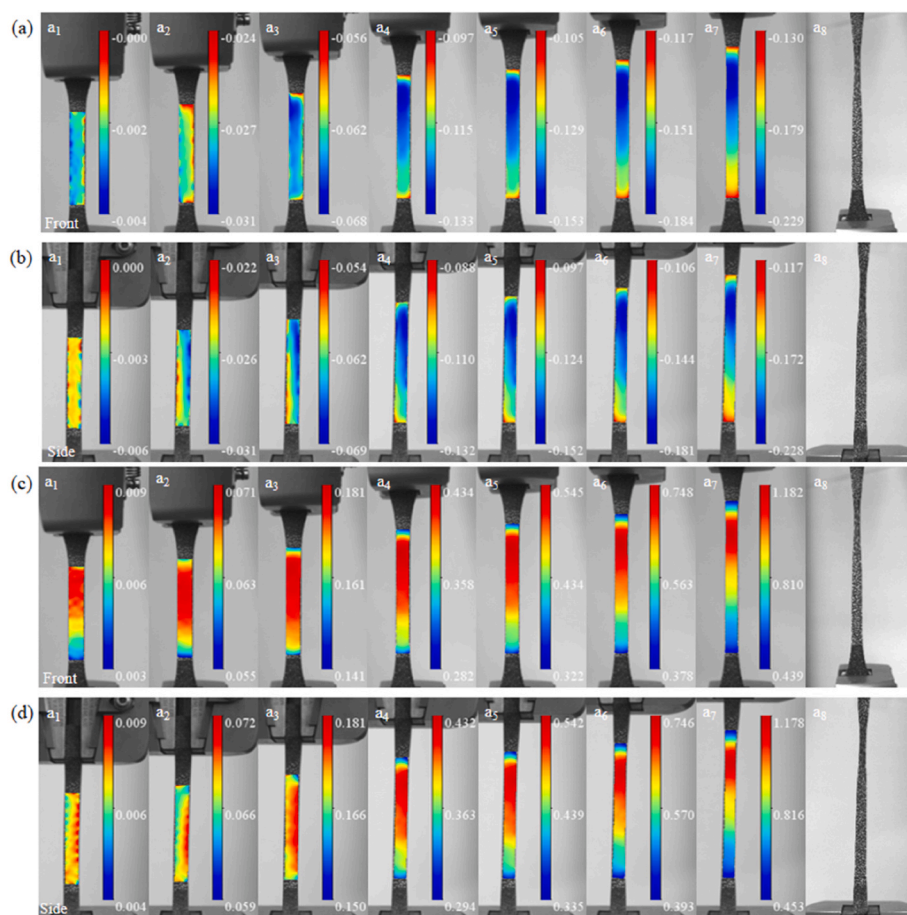Recognizing load and deformation responses is central to describing

Fig. 9. Strain contours of the two perpendicular surfaces of an intact specimen. (a, c) Front and (b, d) side views of the (a, b) horizontal and (c, d) longitudinal strain.
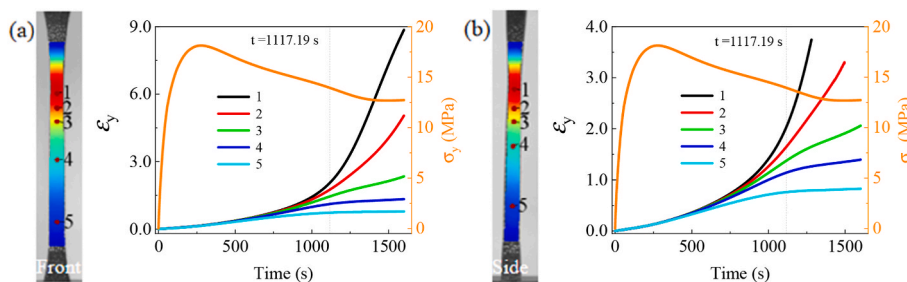

Fig. 10. Time courses of the longitudinal strains at typical areas of intact specimens: (a) front and (b) side view.
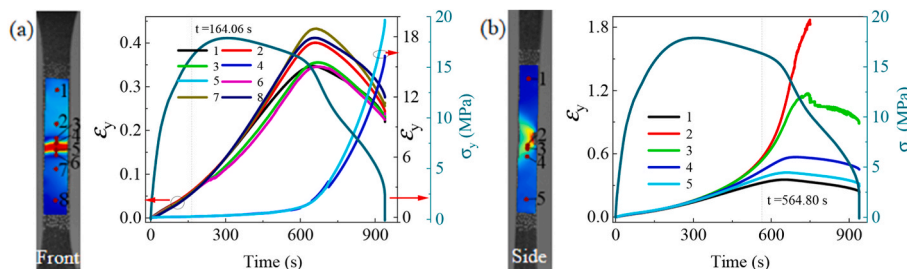

Fig. 11. Time courses of the longitudinal strains at typical areas of pre-cut specimens: (a) front and (b) side view.

and predicting the mechanical behaviors of polymeric materials. Therefore, numerous studies [8,36] have focused on measuring the macroscopic true stress-strain curves to reveal the true behaviors of the necking zone and volumetric strain and understand the macroscopic behaviors of HDPE materials. Our findings revealed the time-course distributions of strain and strain rate at different spatial positions that
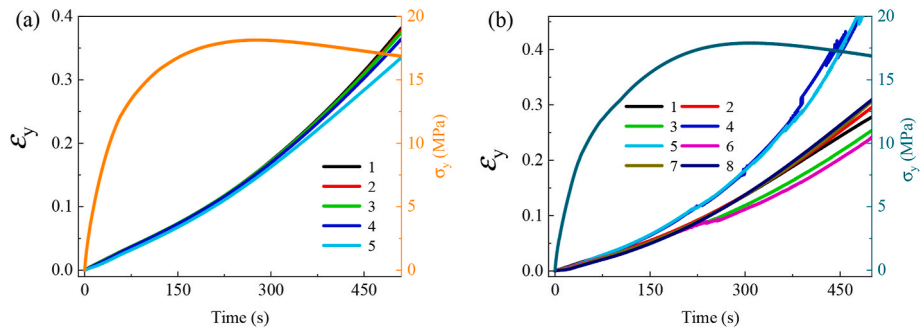
Fig. 12. Magnifications of the early phases of Figs. (a) 10(a) and (b) 11(a).
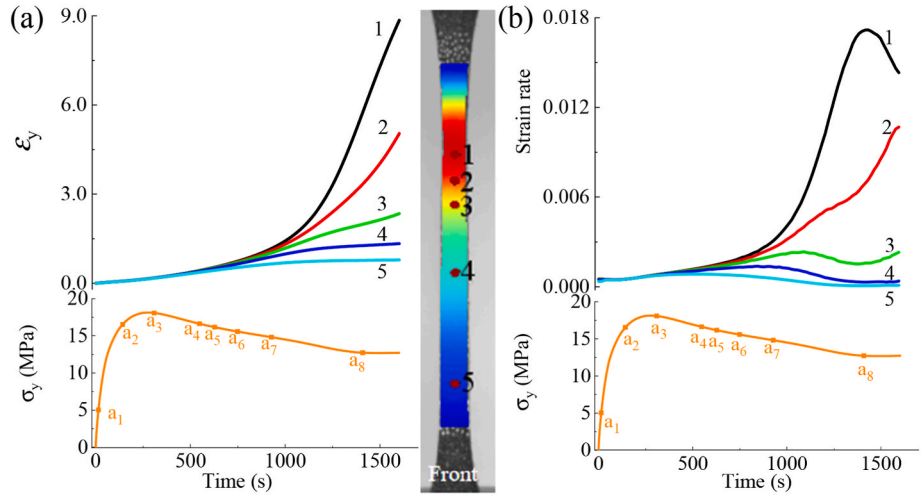

Fig. 13. Front view of an intact specimen (a) Longitudinal strains and stress as functions of time. (b) Stress and rates of the longitudinal strains as functions of time.
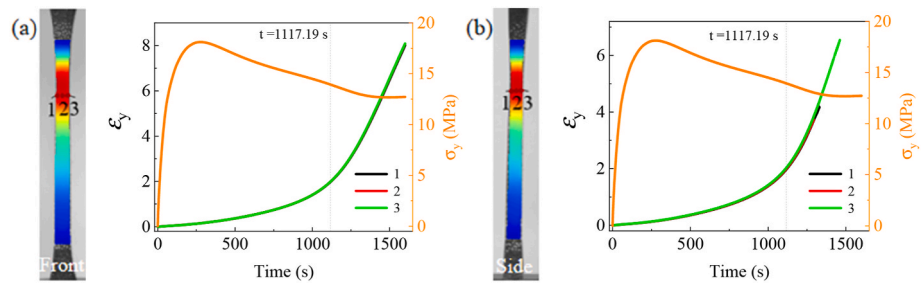

Fig. 14. Time courses of the longitudinal strains in typical areas of an intact specimens: (a) front and (b) side views.
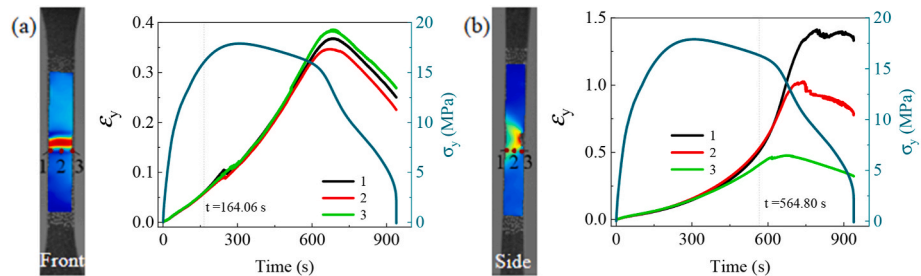
Fig. 15. Time courses of the longitudinal strains in typical areas of a pre-cut specimen: (a) front and (b) side views.

characterized the deformation mechanisms in various phases. The results highlighted the mechanisms of strain field evolution mechanisms corresponding to typical transitions in the macroscopic stress-time curve. These mechanisms are fundamental in constructing an analytical model that describes the behavior of HDPE.

Necking and its propagation are fundamental phenomenon that

occur in polymeric materials. The onset strain point of necking (or strain localization) is generally defined as the (first) peak force point of the load-displacement curve [21,37–41], according to the Considère condition. Our results suggest a novel method of defining the onset strain time of necking and its position, in addition to propagation, based on the spatiotemporal evolving properties of the strains and strain rates. The increases in the local strain rates at all positions accelerate, and no clear strain localizations are observed at the peak force points of the evaluated HDPE specimens. The initiation of necking characterized by the faster increases in the local strain rates in the necked region. In contrast, the strain rates in the regions without necking decelerate. Therefore, our findings suggest a method of predicting necking and its propagation, thus providing a method of evaluating safety by monitoring deformations.

Understanding necking and its propagation is critical in developing an analytical model that describes the behaviors of HDPE and their simulations. Numerous theoretical models [42–44] have been suggested to describe constitutive behaviors considering the necking phenomenon. Microscopic observations indicate that the mechanism of neck propagation (or cold drawing) involves the molecular chains oriented in the tension direction [37,45]. During drawing, the material in the necked region is subjected to a large true stress due to the significant reduction in the cross-sectional area [41]. Strain hardening in the neck zone controls neck propagation [36,42–44,46,47], and the neck regions of polymeric materials propagate when local strengthening in the neck zones due to molecular orientation may compensate for the effects of the decreased cross-sections [37]. Our studies revealed the spatial developments in the time courses of the strains and strain rates with the onset strain of necking and neck propagation. This provided a medium-scale observation between the scale of the molecular chains and that of the macroscopic load-displacement responses. Our findings revealed the mechanism of spatial strain field evolution during necking and neck propagation.

Several areas participated in the neck region, leading to neck propagation. The changes in the strain rates of these areas underwent two transitions: (1) from acceleration to deceleration because of the onset of necking, and (2) from deceleration to acceleration and then these areas underwent necking. These evolving properties are the foundation of mechanical modelling to describe and simulate necking and its propagation.

5.2. Localization and competition between necking and the pre-cut effects

Generally, necking and damage are considered as combined phenomena that lead to strain localization when an HDPE material is under a tension load. A key mechanism of necking (strain localization) is its initiation at the initial defect or weakened point within a solid HDPE material [6,7]. Our results showed that macroscopic cracks diminish neck propagation. This is a significant phenomenon in describing the behaviors of HDPE because it provides a basis to construct a novel model by considering damage-induced and viscoelastic effects on stress-strain behaviors.

In the pre-cut specimen, necking and crack propagation were observed when it was stressed. The competition between necking and pre-cut propagation determines the deformation behaviors and failures of HDPE materials. The strains decreased (recovered) in parts outside the crack zone with crack propagation, which could be attributed to two factors: (1) the pre-crack largely decreased the cross-section at the necking zone and (2) the complicated deformation fields surrounding the crack tip (Fig. 8) severely influenced the orientations of the molecular chains in the necking (strain localization) zone, which limited the strain hardness in this zone. Consequently, the strengthening rate in a the load-bearing capacity of the necking zone could not compensate for its decrease owing to reduction in the cross-section. The second factor was the intrinsic cause of diminishing neck propagation in the intact specimen, because the fracture mode is independent of ligament length

[48]. In contrast, necking in an intact specimen did not induce unloading of outside zones (Fig. 9) although their strain rates decelerated (Fig. 13), such that necking increased with elongation. Consequently, these results highlight a method of defining a crack zone based on strain evolutions and thus suggests a possible method of predicting failure.

Decreases in deformation (recoveries) were observed in the horizontal and vertical components of the strains in the pre-cut specimen. The recoveries of the horizontal strains indicated transitions from compact to expansion in these zones. This limited neck propagation along the length of the pre-cut specimen.

6. Conclusions

The spatial distributions of the time courses of the strains and strain rates revealed the spatiotemporal strain field evolution, which induced necks and fractures in HDPE materials under tension. These findings highlight in the changes in the strain field patterns of evolution in intact and pre-cut specimens under tension and the effects of pre-cutting.

(1) These two types of specimens exhibited heterogeneous evolution patterns in terms of their time courses of strains and strain rates at different spatial positions. In the intact specimen, following the earlier linear evolutions with time, three types of strain rate evolutions were observed at different positions: (i) in the nucleation zone of necking, the strain rates transitioned to acceleration and finally to deceleration until failure; (ii) in the propagation zone of necking, the strain rate initially transitioned to acceleration and then deceleration because of necking in the nucleation zone, followed by acceleration and participation in the necking zone; and (iii) at zones far from the necking zone, the strain rates transitioned to acceleration and then deceleration until stabilization at a constant strain state.

(2) In the pre-cut specimen, after the earlier linear stage and the subsequent accelerations of the strain evolutions, two types of strain patterns were observed in the fracture and outside zones, respectively: (i) in the fracture zone, the strain rates continuously accelerated until failure; and (ii) in the outside zones, the strains decreased after reaching maxima. Thus, these positions released their stored deformation energies.

(3) Energy release from positions outside the crack zone caused the macroscopic stress-strain curve of the pre-cut specimen to deviate from that of an intact specimen. Necking and its propagation in the tension direction dominated the failure behavior of the intact specimen. However, the failure of the pre-cut specimen was dominated by crack propagation, which prevented neck propagation.

(4) Before the stress reached its (first) peak point, the surface strains of both specimens displayed almost homogeneously spatial distributions, and the strains at all positions exhibited linear time courses. Subsequently, the time courses of the strains at all positions exhibited acceleration.

(5) The onset strain of necking may be defined as the faster increase in the strain rate at the necking nucleation zone. In contrast, the strain rates or their accelerations at other positions decrease.

CRediT authorship contribution statement

Shengwang Hao: Funding acquisition, Formal analysis, Conceptualization, Project administration, Supervision, Writing – review & editing. **Xinyue Wu:** Formal analysis, Conceptualization, Investigation, Methodology, Writing – original draft. **Chunsheng Lu:** Formal analysis, Supervision, Writing – review & editing.

Declaration of competing interest

The authors declare that they have no known competing financial interests or personal relationships that could have appeared to influence the work reported in this paper.

Data availability

Data will be made available on request.

References

[1] R.N. Haward, The Physics of Glassy Polymers, Applied Science Publishers, London, 1973.

[2] R. Séguéla, On the natural draw ratio of semi-crystalline polymers: review of the mechanical, physical and molecular aspects, Macromol. Mater. Eng. 292 (3) (2007) 235–244.

[3] S. Humbert, O. Lame, G. Vigier, Polyethylene yielding behaviour: what is behind the correlation between yield stress and crystallinity? Polymer 50 (15) (2009) 3755–3761.

[4] B. Xiong, O. Lame, C. Jean-Marc, Y. Men, G. Vigier, Critical stress and thermal activation of crystal plasticity in polyethylene: influence of crystal microstructure and chain topology, Polymer 118 (2017) 192–200.

[5] Y. Men, Critical strains determine the tensile deformation mechanism in semicrystalline polymers, Macromolecules 53 (21) (2020) 9155–9157.

[6] H. Guo, R.G. Rinaldi, M. Broudin, S. Tayakout, O. Lame, Anisotropic deformation and failure behaviors of the necked HDPE materials induced by oligo-cyclic loading, Polymer 234 (2021), 124232.

[7] J. Ye, S. André, L. Farge, Kinematic study of necking in a semi-crystalline polymer through 3D digital image correlation, Int. J. Solid Struct. 59 (2015) 58–72.

[8] E.M. Parsons, M.C. Boyce, D.M. Parks, M. Weinberg, Three-dimensional large-strain tensile deformation of neat and calcium carbonate-filled high-density polyethylene, Polymer 46 (7) (2005) 2257–2265.

[9] G. Mirone, The dynamic effect of necking in Hopkinson bar tension tests, Mech. Mater. 58 (2013) 84–96.

[10] L.H. Zhang, G. Gour, N. Petrinic, A. Pellegrino, Rate dependent behaviour and dynamic strain localisation of three novel impact resilient titanium alloys: experiments and modelling, Mat. Sci. Eng. A-Struct. 771 (2020), 138552.

[11] S.W. Hao, H.Y. Wang, M.F. Xia, F.J. Ke, Y.L. Bai, Relationship between strain localization and catastrophic rupture, Theor. Appl. Fract. Mech. 48 (1) (2007) 41–49.

[12] H. Zhang, G.Y. Huang, H.P. Song, Y.L. Kang, Experimental characterization of strain localization in rock, Geophys. J. Int. 194 (3) (2013) 1554–1558.

[13] Q.Z. Fang, T.J. Wang, H.M. Li, Large tensile deformation behavior of PC/ABS alloy, Polymer 47 (14) (2006) 5174–5181.

[14] O. De Almeida, F. Lagattu, J. Brillaud, Analysis by a 3D DIC technique of volumetric deformation gradients: application to polypropylene/EPR/talc composites, Compos. Part A-Appl. S. 39 (8) (2008) 1210–1217.

[15] Y.G. Han, A.D. Rogalsky, B.X. Zhao, H.J. Kwon, The application of digital image techniques to determine the large stress-strain behaviors of soft materials, Polym. Eng. Sci. 52 (4) (2012) 826–834.

[16] C.P. Goh, H. Ismail, K.S. Yen, M.M. Ratnam, Single-step scanner-based digital image correlation (SB-DIC) method for large deformation mapping in rubber, Opt Laser. Eng. 88 (2017) 167–177.

[17] S. Agnelli, W. Balasooriya, F. Bignotti, B. Schrittesser, On the experimental measurement of fracture toughness in SENT rubber specimens, Polym. Test. 87 (2020).

[18] F. Grytten, H. Daiyan, M. Polanco-Loria, S. Dumoulin, Use of digital image correlation to measure large-strain tensile properties of ductile thermoplastics, Polym. Test. 28 (6) (2009) 653–660.

[19] B. Pan, D.F. Wu, Y. Xia, Incremental calculation for large deformation measurement using reliability-guided digital image correlation, Opt Laser. Eng. 50 (4) (2012) 586–592.

[20] Y.H. Zhou, C. Sun, J.B. Chen, Adaptive subset offset for systematic error reduction in incremental digital image correlation, Opt Laser. Eng. 55 (2014) 5–11.

[21] C. G'Sell, J.M. Hiver, A. Dahoun, Experimental characterization of deformation damage in solid polymers under tension, and its interrelation with necking, Int. J. Solid Struct. 39 (13–14) (2002) 3857–3872.

[22] F. Addiego, A. Dahoun, C.G." Sell, J.M. Hiver, Characterization of volume strain at large deformation under uniaxial tension in high-density polyethylene, Polymer 47 (12) (2006) 4387–4399.

[23] A.L. Bowman, S. Mun, B.D. Huddleston, S.R. Gwaltney, M.I. Baskes, M.F. Horstemeyer, A nanoscale study of size scale, strain rate, temperature, and stress state effects on damage and fracture of polyethylene, Mech. Mater. 161 (2021), 104008.

[24] C.G." Sell, A. Dahoun, Evolution of microstructure in semi-crystalline polymers under large plastic deformation, Mater. Sci. Eng., A 175 (1–2) (1994) 183–199.

[25] Z. Bartczak, A. Galeski, A.S. Argon, R.E. Cohen, On the plastic deformation of the amorphous component in semicrystalline polymers, Polymer 37 (11) (1996) 2113–2123.

[26] F. Addiego, A. Dahoun, C. G'Sell, J.-M. Hiver, O. Godard, Effect of microstructure on crazing onset in polyethylene under tension, Polym. Eng. Sci. 49 (6) (2009) 1198–1205.

[27] R.A.C. Deblieck, D.J.M. van Beek, K. Remerie, I.M. Ward, Failure mechanisms in polyolefines: the role of crazing, shear yielding and the entanglement network, Polymer 52 (14) (2011) 2979–2990.

[28] F. Rezgui, C. G'Sell, A. Dahoun, J.M. Hiver, T. Sadoun, Plastic deformation of low-density polyethylene reinforced with biodegradable polylactide, part 1: microstructural analysis and tensile behavior at constant true strain-rate, Polym. Eng. Sci. 51 (1) (2011) 117–125.

[29] ISO 18489 Polyethylene (PE) Materials for Piping Systems-Determination of Resistance to Slow Crack Growth under Cyclic Loading-Cracked Round Bar Test Method, International Organization for Stardization, Geneva, Switzerland, 2015.

[30] M. Thuy, M. Pedragosa-Rincon, U. Niebergall, H. Oehler, I. Alig, M. Bohning, Environmental stress cracking of high-density polyethylene applying linear elastic fracture mechanics, Polymers 14 (12) (2022).

[31] G. Lewis, Apparent fracture toughness of acrylic bone cement: effect of test specimen configuration and sterilization method, Biomaterials 20 (1) (1999) 69–78.

[32] Y.H. Xiao, D.A. Rennerfeldt, E.A. Friis, S.H. Gehrke, M.S. Detamore, Evaluation of apparent fracture toughness of articular cartilage and hydrogels, J. Tissue Eng. Regener. Med. 11 (1) (2017) 121–128.

[33] J. Hyon, O. Lawal, O. Fried, R. Thevamaran, S. Yazdi, M.J. Zhou, D. Veysset, S.E. Kooi, Y. Jiao, M.S. Hsiao, J. Streit, R.A. Vaia, E.L. Thomas, Extreme energy absorption in glassy polymer thin films by supersonic micro-projectile impact, Mater. Today 21 (8) (2018) 817–824.

[34] I.C. Yeh, J.W. Andzelm, G.C. Rutledge, Mechanical and structural characterization of semicrystalline polyethylene under tensile deformation by molecular dynamics simulations, Macromolecules 48 (12) (2015) 4228–4239.

[35] GB/T 8804, 3-2003. Thermoplastic Pipes-Determination of Tensile Properties-Part 3: Polyolefin Pipes, China Standard Press, Beijing, 2003.

[36] P.D. Coates, I.M. Ward, The plastic deformation behaviour of linear polyethylene and polyoxymethylene, J. Mater. Sci. 13 (9) (1978) 1957–1970.

[37] A. Peterlin, Molecular model of drawing polyethylene and polypropylene, J. Mater. Sci. 6 (6) (1971) 490–508.

[38] C. G'Sell, N.A. Aly-Helal, J.J. Jonas, Effect of stress triaxiality on neck propagation during the tensile stretching of solid polymers, J. Mater. Sci. 18 (6) (1983) 1731–1742.

[39] P. Tugcu, K.W. Neale, Approximate methods for analysing the cold drawing of polymeric fibres and films, Int. J. Numer. Methods Eng. 25 (1) (1988) 95–112.

[40] P. Tugcu, K.W. Neale, Analysis of neck propagation in polymeric fibres including the effects of viscoplasticity, J. Eng. Mater. Technol. 110 (4) (1988) 395–400.

[41] B. Crist, C. Metaxas, Neck propagation in polyethylene, J. Polym. Sci., Polym. Phys. Ed. 42 (11) (2004) 2081–2091.

[42] J.W. Hutchinson, J.P. Miles, Bifurcation analysis of the onset of necking in an elastic/plastic cylinder under uniaxial tension, J. Mech. Phys. Solid. 22 (1) (1974) 61–71.

[43] J.W. Hutchinson, K.W. Neale, Neck propagation, J. Mech. Phys. Solid. 31 (5) (1983) 405–426.

[44] R.G. Ramachandran, R. Maiti, S.S. Velankar, Necking and drawing of rubber-plastic laminate composites: finite element simulations and analytical model, J. Mech. Phys. Solid. 142 (2020), 104012.

[45] J.M. Andrews, I.M. Ward, The cold-drawing of high density polyethylene, J. Mater. Sci. 5 (5) (1970) 411–417.

[46] D.M. Bigg, A review of techniques for processing ultra-high modulus polymers, Polym. Eng. Sci. 16 (11) (1976) 725–734.

[47] P.D. Coates, I.M. Ward, Neck profiles in drawn linear polyethylene, J. Mater. Sci. 15 (11) (1980) 2897–2914.

[48] M. Elmeguenni, M. Nait-Abdelaziz, F. Zairi, J.M. Gloaguen, Fracture characterization of high-density polyethylene pipe materials using the J-integral and the essential work of fracture, Int. J. Fract. 183 (2) (2013) 119–133.